Similarity Renormalization Groups (SRG) for nuclear forces

Nuclear structure and nuclear astrophysics

Philipp Dijkstal

12.05.2016

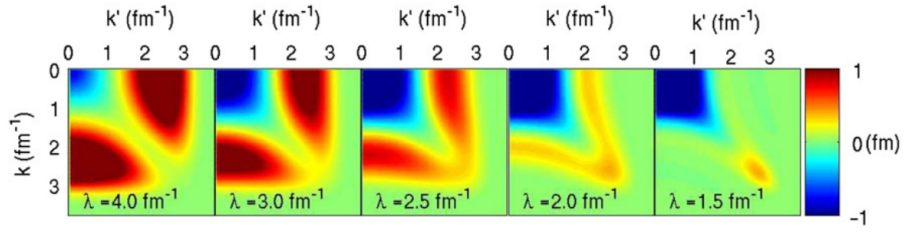

1 Introduction

The talk on Similarity Renormalization Groups (SRG) from the seminar on nuclear structure and nuclear astrophysics is brought to written form here. It begins with a short introduction to the basics of low energy nuclear forces before outlining the shortcomings of phenomenological potentials such as Argonne ν_{18}. The large computational efforts that have to be taken in nuclear physics calculations serve as a motivation for Renormalization Groups. The principles of SRG are then explained and a basic flow equation is derived. The induced amplification of 3-body forces and higher are discussed. The results of several calculations that use SRG evolved potentials are presented. Unresolved problems lie within the higher order forces.

2 Potentials in low-energy nuclear physics

The theory of low-energy nuclear physics is used to describe the structure and behavior of nuclei. Figure 1 gives an overview of the energy scales for different degrees of freedom in nuclear physics.

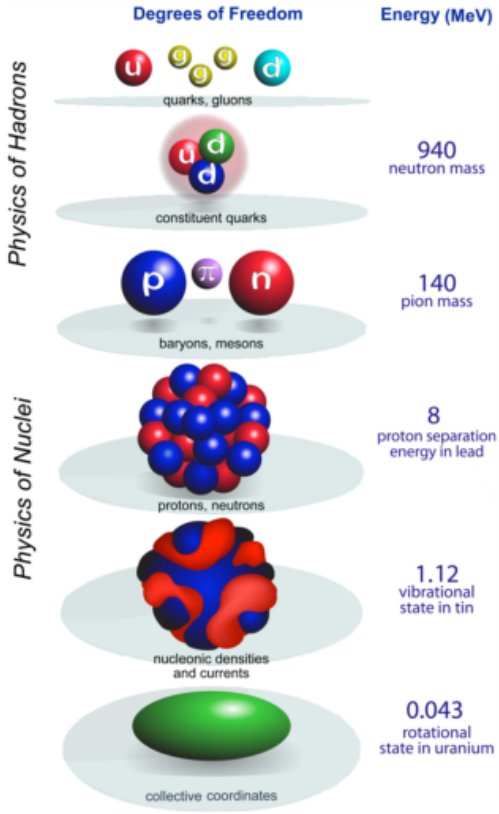

Figure 1: Depending on the energy scale of interest, the relevant degrees of freedom change. For low energy nuclear physiscs, a typical energy scale is 200 MeV [1].

Since the typical momentum within large nuclei is around 200 MeV, the relevant degrees of freedom are neutrons and protons with the pion as an exchange particle. The forces between nucleons are described by potentials. As an example, Fig. 2 (left) shows several phenomenological potentials for the $^1S_0$ scattering channel in position representation. These potentials were directly fit to experiment data and are purely local, which means they only depend on the relative distance between the nucleons. Several properties are notable:

- A strong repulsive core at short distances.
- The long ranged part of the potential is attractive.
- The potentials look quite different, especially Bonn and AV18, yet they still reproduce the experimental data.

Since nuclear physics calculations are usually performed in momentum space, Fig. 2 (right) shows the Fourier transformed Argonne ν_{18} potential. To better understand the axes it is helpful to know that k and k' are the relative momenta before and after the scattering and that 1 fm^{-1} corresponds to an energy of about 200 MeV. This is, as it was stated before, roughly the energy that is important within nuclei. A close look at the potential shows very high contributions at the off-diagonal high energy parts. These correspond to the repulsive core and are inconvenient for many calculations. This is demonstrated by means of the T matrix that is used to calculate scattering phase shifts:

$$T_l(k,k',E) = V_l(k,k') + \tag{1}$$

$$\frac{2}{\pi}\int q^2 \mathrm{d}q \frac{V_l(k,q)T_l(q,k',E)}{E - q^2/2\mu + i\epsilon} \tag{2}$$

It is clear that even if T is only evaluated for small k, the off-diagonal elements contribute. It would be much better if $V(k,k')$ had a close to diagonal shape as this would decouple low from high momenta and allow for a truncation. Similarity Renormalization Groups as they are introduced next are used to transform potentials in this way.

3 Similarity Renormalization Groups

3.1 Flow equation

Basis transformations by insertion of a $\mathbb{1}$ are commonly used in quantum mechanics:

$$E = \langle\Psi|H|\Psi\rangle = \langle\Psi|\underbrace{U^\dagger U}_{\mathbb{1}} HU^\dagger U|\Psi\rangle \tag{3}$$

$$= \langle\widetilde{\Psi}|\widetilde{H}|\widetilde{\Psi}\rangle \tag{4}$$

With a good choice of U, an effect as schemed in the title image of this report can be achieved - the reduction of off-diagonal matrix elements in favor of on-diagonal elements. $\widetilde{H}$ should be found by a steady evolution, indicated by a scale parameter s (H_s). This means that $H_0 = H$. A flow equation is now derived to obtain a differential equation for H_s.

$$H_s = U_s H U_s^\dagger \tag{5}$$

The next couple of steps lead to a more convenient form and introduce the operator η_s instead of U_s.

$$\tag{6}$$

$$\frac{\mathrm{d}H_s}{\mathrm{d}s} = \frac{\mathrm{d}U_s}{\mathrm{d}s} HU_s^\dagger + U_s H \frac{\mathrm{d}U_s^\dagger}{\mathrm{d}s} \tag{7}$$

$$= \frac{\mathrm{d}U_s}{\mathrm{d}s}\underbrace{U_s^\dagger U_s}_{\mathbb{1}} HU_s^\dagger + \underbrace{U_s H U_s^\dagger}_{H_s} U_s \frac{\mathrm{d}U_s^\dagger}{\mathrm{d}s} \tag{8}$$

$$= \eta_s H_s + H_s \eta_s^\dagger = [\eta_s, H_s] \tag{9}$$

$$\eta_s = \frac{\mathrm{d}U_s}{\mathrm{d}s} U_s^\dagger = -\eta_s^\dagger \tag{10}$$

Now, η_s is expressed with a generator G_s to ensure the behavior as demanded in the previous equation.

$$\eta_s = [G_s, H_s] \tag{11}$$

$$\frac{\mathrm{d}H_s}{\mathrm{d}s} = [[G_s, H_s], H_s] \tag{12}$$

$$= G_s H_s H_s - 2H_s G_s H_s + H_s H_s G_s \tag{13}$$

At this point, the most common choice of $G_s = T$ is used. This is obviously convenient for calculations in momentum space as T is diagonal in this basis, with $T|k\rangle = \epsilon_k|k\rangle$. Moreover it has the effect that only the potential is changed during the evolution:

$$\frac{\mathrm{d}H_s}{\mathrm{d}s} = \frac{\mathrm{d}V_s}{\mathrm{d}s} \tag{14}$$

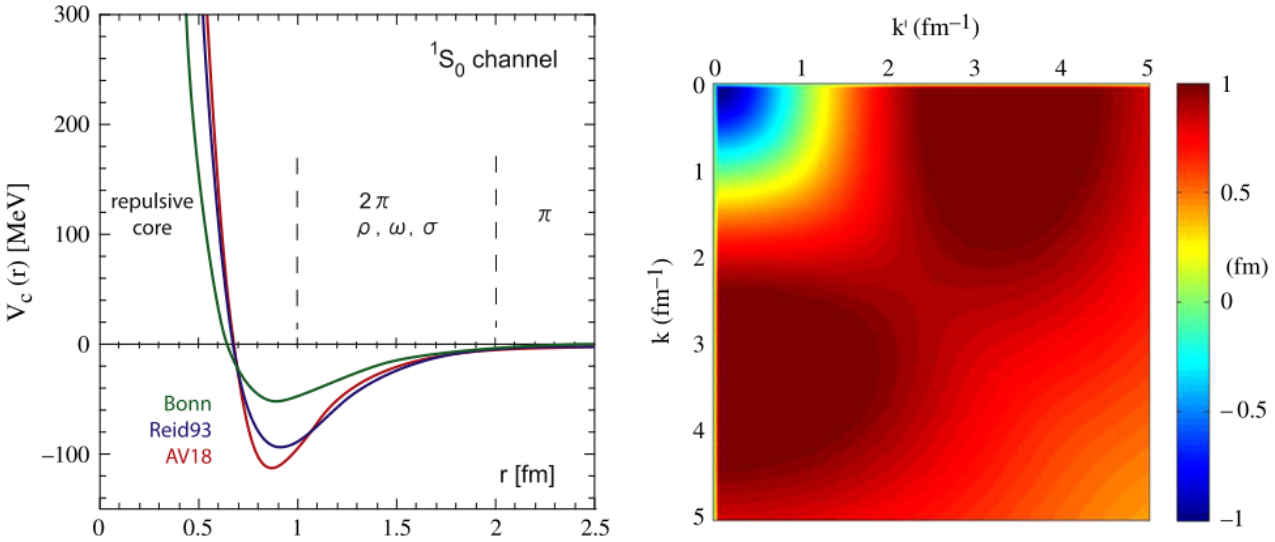

Figure 2: The left plot shows several phenomenological potentials in position representation. On the right, it is the Argonne ν_{18} potential in momentum representation. 1 fm^{-1} corresponds to about 200 MeV [1].

With $H_s = T + V_s$, Eq. (13) can be expanded to evaluate the matrix elements of $\mathrm{d}V_s/\mathrm{d}s$.

$$\frac{\mathrm{d}V_s}{\mathrm{d}s} = 2(TV_sT - V_sTV_s) + V_s^2T + TV_s^2 - V_sT^2 - T^2V_s \qquad (15)$$

A $\mathbb{1} = \frac{2}{\pi}\int q^2\mathrm{d}q$ has to be inserted within the summands that include V_s^2.

$$\frac{\mathrm{d}V_s}{\mathrm{d}s}(k,k') = \langle k'|V_s|k\rangle \qquad (16)$$

$$= -(\epsilon_k'^2 - \epsilon_k)^2 V(k,k') + \frac{2}{\pi}\int_0^\infty q^2\mathrm{d}q(\epsilon_k + \epsilon_{k'} - 2\epsilon_q)V_s(k,q)V_s(q,k') \qquad (17)$$

The last equation includes two terms, the first of which results in an exponential decrease of off-diagonal elements as V is evolved. If V_s is small, the second term can be seen as a second order correction. Otherwise the behavior of Eq. (17) is not clear, however the first term evidently dominates in practise [2].

3.2 Examples of SRG

As an example, Fig. 3 (top) shows the $^3S_1$ channel of the Argonne potential as it is evolved with SRG. Instead of s, $\lambda = {}^1/_{s^{1/4}}$ is used as the flow parameter. The transformation to a rather diagonal form is nicely visible. Below that in Fig. 3, the same potential in position space is shown together with an EFT potential. Note that the evolved potential is no longer local, therefore the projected potential $\bar{V}(r)$ is given:

$$\bar{V}(r) \propto \int \mathrm{d}r' V(r,r') \qquad (18)$$

One can see that the repulsive core of the ν_{18} potential is removed during the process and the potentials are a lot smoother.

Such evolved potentials have the power to greatly improve multi-body calculations, for example within the scope of the No Core Shell Model (NCSM). Only the basic idea of NCSM shall be stated here. It is used to calculate ground state energies of light nuclei. These are modelled by protons and neutrons in an harmonic oscillator basis. Since the distribution of nucleons into $\mathrm{N_{max}}$ shells is a combinatorial problem, the number of possibilities grows rapidly as more shells are added (Fig. 4 left). These possibilities form the basis of NCSM calculations and determine the size of the matrices that have to bi diagonalized. Today's computational power limits the matrix size to about 10^9, therefore it is important that calculations converge for a smaller $\mathrm{N_{max}}$ [3]. NCSM uses nucleon potentials as an input. In Fig. 4 (right), it can be seen how SRG evolved potentials show a fast convergence, whereas calculations using the original potential are not successful.

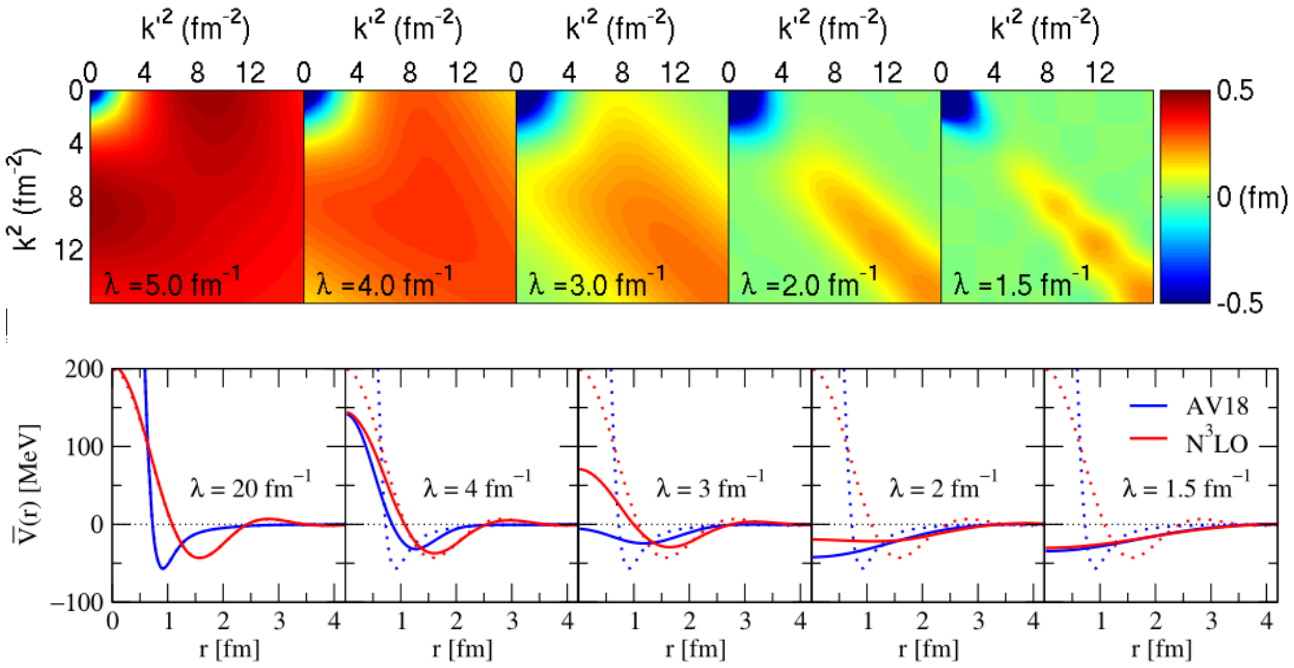

Figure 3: Top: The Argonne ν_{18} potential in the $3S_1$ channel is evolved with SRG. Bottom: The local projections of the ν_{18} and a higher order contribution to an EFT potential are shown. The effects of SRG can be seen in both plots [1].

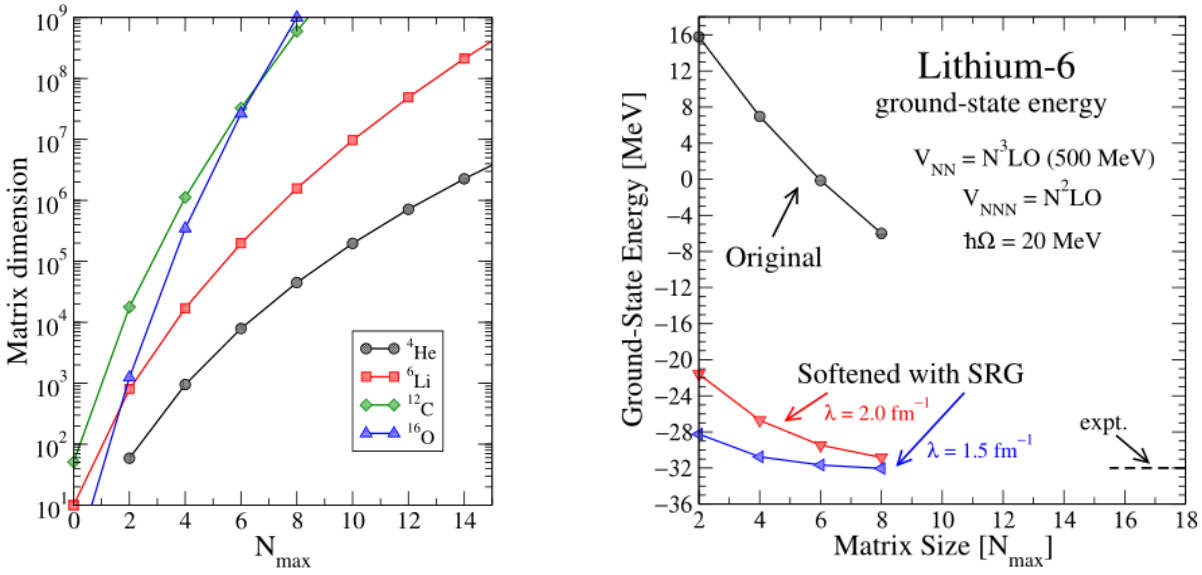

Figure 4: Left: The dimension of matrices that occur in NCSM calculations for selected nuclei depending on the number of available shells. Matrices larger than 10^9 cannot be diagonalized with nowadays computational possibilities. Right: Calculations for ^{6}Li using a SRG evolved potential converge and yield a ground state energy close to experimental results [1].

4 Multi-body forces

Multi-body forces are being induced and amplified by SRG, which leads to difficulties and prevents an exorbitant evolution. Before providing an explanation, the origin of such forces in chiral EFT is raised for a more systematic approach. Figure 5 shows the force hierarchy as an expansion of the momentum Q over the cutoff λ. The cutoff is roughly the mass of the next not considered degree of freedom. The expansion begins with momentum independent contact interactions and pion exchanges in leading order (LO). Three-body forces appear naturally in chiral EFT as a consequence of neglected higher degrees of freedom. A more detailed discussion of EFT is beyond the scope of this report, but can be found for example in [2].

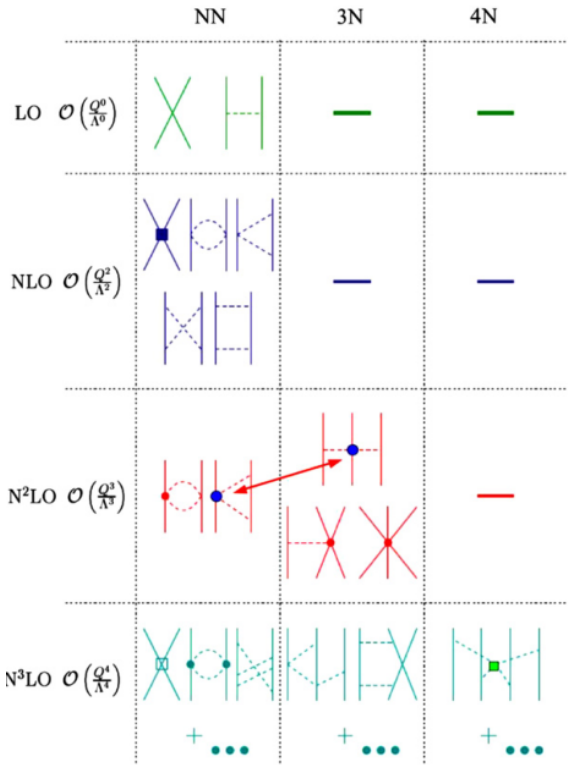

Figure 5: The hierarchy of forces in chiral EFT. Feynman diagrams scheme the various kinds of interactions [2].

How SRG induces multi-body forces can easily be understood from the flow equation (Eq. 12) in second quantization. G is taken to be a one-body operator however it is not restricted to T. The original potential is assumed to contain no higher than two-body forces and is therefore denoted H_{NN}. If the commutators are multiplied out and brought back to normal ordering (all constructors to the left), then the derivative of H_{NN} also contains 3-body forces and higher.

$$\frac{\mathrm{d}H_s}{\mathrm{d}s} = [[G, H_{NN}], H_{NN}] \tag{19}$$

$$= \underbrace{\sum a^\dagger a^\dagger a a}_{\text{2 body}} + \underbrace{\sum a^\dagger a^\dagger a^\dagger a a a}_{\text{3 body}} + \ldots \tag{20}$$

The unitarity of the SRG evolution is therefore only preserved if all these higher order forces are considerd. In practise however, most calculations have to be truncated after the inclusion of 3-body forces. This therefore puts a limit on the extent of the SRG evolution, at some point it has to be stopped.

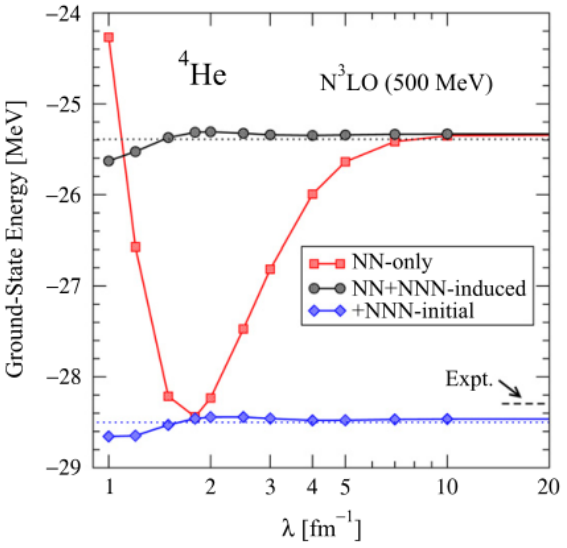

Figure 6: This plot shows the consequences of neglecting the induced 3-body forces and the importance of 4-body forces for a NCSM calculation of the ^{4}He binding energy. The evolution of the potentials takes place from right to left [1].

The importance of the induced 3-body force is illustrated in Fig. 6. It shows a NCSM calculation of the ^{4}He binding energy. The potentials that are used here are being evolved with SRG to find out whether the result changes.

- If the induced 3-body force is neglected after starting with a NN-potential, convergence is lost immediately (red curve).
- If it is considered however, the energy remains almost unchanged for quite some time

(blue curve).

- If 3-body forces are part of the potential from the beginning, the convergence behavior is the same (blue curve). In this case, the results are much closer to the experimental value.
- The significance of 4-body forces is a possible explanation for the remaining disagreement.

5 Heavy nuclei

After showing applications of SRG for lighter nuclei (Fig. 6 and 4), the status of the calculations for heavy nuclei is now regarded. NCSM can only be applied to nuclei with mass numbers of about 24 or lower, whereas CC is better suited beyond [3].

Figure 8 shows some Coupled Cluster (CC) calculations for nuclei with mass numbers between 16 and 132. The error bars cover the change of the result as the evolution parameter is varied within reasonable limits, while the arrows indicate the direction of the change. It is clear that these calculations are not accurate yet as the differences to the experimental results are high. In order to improve them, the higher order forces have to be understood and handled better which is a task of current research also at the TU Darmstadt.

6 Comparison of CC to NCSM

The next plot in Fig. 7 shows that the results from the multi-body methods CC and NCSM are very similar, even though they model the nucleus in a very different way. Once again however the bottom part of the plot shows that the higher order forces represent an unsolved problem since there is no convergence if the 3-body forces are accounted for from the start.

On the bright side this comparison is an indication that the calculation methods themselves are trustworthy whereas the problems lie within the nucleon potentials that serve as an input to these methods.

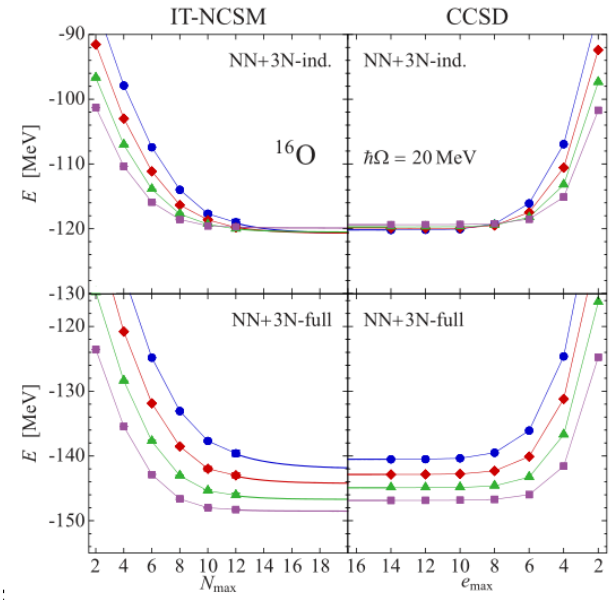

Figure 7: CC and NCSM show very similar results for the ground state energy of ^{16}O. The colors indicate the change of the flow parameter from 0.04 fm^4 (blue) until 0.08 fm^4 (purple) [4].

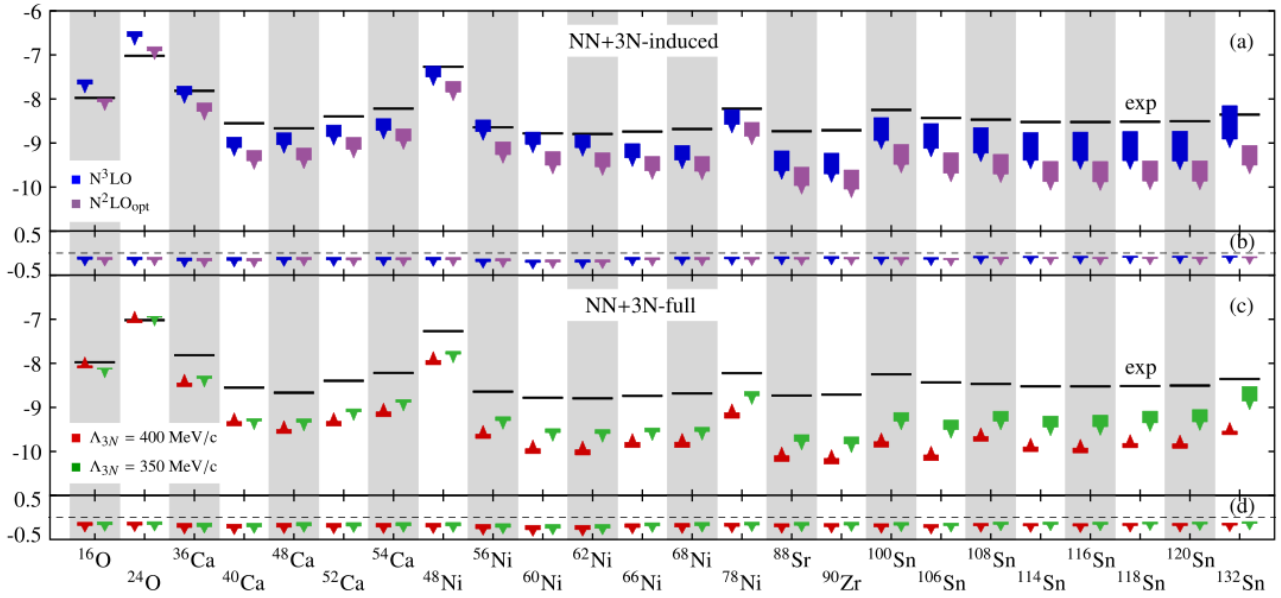

Figure 8: Ground state energies per nucleon in MeV for heavy nuclei with Coupled Cluster (CC) calculations. The subplots (b) and (d) show the contribution of the triple correction which is not of interest here [5].

References

[1] R. Furnstahl, The renormalization group in nuclear physics, Nuclear Physics B - Proceedings Supplements 228 (2012) 139 – 175.

[2] S. Bogner, R. Furnstahl, A. Schwenk, From low-momentum interactions to nuclear structure, Progress in Particle and Nuclear Physics 65 (1) (2010) 94 – 147.

[3] A. Schwenk, Nuclear physics, Lecture notes (2016).

[4] R. J. Furnstahl, K. Hebeler, New applications of renormalization group methods in nuclear physics, Reports on Progress in Physics 76 (12) (2013) 126301.

[5] S. Binder, J. Langhammer, A. Calci, R. Roth, Ab initio path to heavy nuclei, Physics Letters B 736 (2014) 119 – 123.